Acta Pharmaceutica Sinica B 2024;14(4):1772−1786

Chinese Pharmaceutical Association
Institute of Materia Medica, Chinese Academy of Medical Sciences

Acta Pharmaceutica Sinica B

www.elsevier.com/locate/apsb
www.sciencedirect.com

ORIGINAL ARTICLE

High-throughput discovery of highly selective reversible hMAO-B inhibitors based on at-line nanofractionation

Yu Fan[a,†], Jincai Wang[a,†], Jingyi Jian[a,b,†], Yalei Wen[a], Jiahao Li[a], Hao Tian[a], Jacques Crommen[c], Wei Bi[d,*], Tingting Zhang[a,*], Zhengjin Jiang[a,*]

[a]*Institute of Pharmaceutical Analysis/Guangdong Province Key Laboratory of Pharmacodynamic Constituents of TCM and New Drugs Research/International Cooperative Laboratory of Traditional Chinese Medicine Modernization and Innovative Drug Development of Ministry of Education (MOE) of China/College of Pharmacy, Jinan University, Guangzhou 510632, China*
[b]*KU Leuven-University of Leuven, Pharmaceutical Analysis, Department of Pharmaceutical and Pharmacological Sciences, Leuven 3000, Belgium*
[c]*Laboratory of Analytical Pharmaceutical Chemistry, Department of Pharmaceutical Sciences, CIRM, University of Liege, Liege B-4000, Belgium*
[d]*Department of Neurology, the First Affiliated Hospital of Jinan University/Clinical Neuroscience Institute, the First Affiliated Hospital of Jinan University, Guangzhou 510630, China*

Received 15 December 2023; received in revised form 11 January 2024; accepted 29 January 2024

KEY WORDS

Human monoamine oxidase B inhibitors;
High-throughput screening;
At-line nanofractionation;
Parkinson's disease;
Cellular neuroprotection;
Traditional Chinese medicines (TCMs)

Abstract Human monoamine oxidase B (hMAO-B) has emerged as a pivotal therapeutic target for Parkinson's disease. Due to adverse effects and shortage of commercial drugs, there is a need for novel, highly selective, and reversible hMAO-B inhibitors with good blood-brain barrier permeability. In this study, a high-throughput at-line nanofractionation screening platform was established with extracts from Chuanxiong Rhizoma, which resulted in the discovery of 75 active compounds, including phenolic acids, volatile oils, and phthalides, two of which were highly selective novel natural phthalide hMAO-B inhibitors that were potent, selective, reversible and had good blood−brain permeability. Molecular docking and molecular dynamics simulations elucidated the inhibition mechanism. Sedanolide (IC_{50} = 103 nmol/L; SI = 645) and neocnidilide (IC_{50} = 131 nmol/L; SI = 207) demonstrated their excellent potential as hMAO-B inhibitors. They offset the limitations of deactivating enzymes associated with irreversible

*Corresponding authors.
E-mail addresses: biwei4762@sina.com (Wei Bi), tzhtt008@jnu.edu.cn (Tingting Zhang), jzjjackson@hotmail.com (Zhengjin Jiang).
[†]These authors made equal contributions to this work.
Peer review under the responsibility of Chinese Pharmaceutical Association and Institute of Materia Medica, Chinese Academy of Medical Sciences.

https://doi.org/10.1016/j.apsb.2024.01.020

hMAO-B inhibitors such as rasagiline. In SH-SY5Y cell assays, sedanolide (EC_{50} = 0.962 μmol/L) and neocnidilide (EC_{50} = 1.161 μmol/L) exhibited significant neuroprotective effects, comparable to the positive drugs rasagiline (EC_{50} = 0.896 μmol/L) and safinamide (EC_{50} = 1.079 μmol/L). These findings underscore the potential of sedanolide as a novel natural hMAO-B inhibitor that warrants further development as a promising drug candidate.

1. Introduction

Parkinson's disease (PD), the second most common neurodegenerative disease after Alzheimer's disease (AD), affects over 6 million people worldwide, with China accounting for 50%[1]. Monoamine oxidases (MAOs) play a role in the homeostasis of the healthy brain and are altered in various disease states. There are two isoforms of MAOs, MAO-A and MAO-B, with human MAO-B (hMAO-B) recognized as a therapeutic target for neurodegenerative diseases including PD[2] and AD[3]. MAO-B is located on the outer mitochondrial membrane and is responsible for dopamine, serotonin, and norepinephrine degradation, as well as being involved in oxidative stress and apoptosis[4]. Selegiline, rasagiline, and safinamide are classic commercial enzyme inhibitor drugs used for PD treatment, exerting neuroprotective effects by inhibiting hMAO-B[5−7]. Safinamide, a third-generation reversible hMAO-B inhibitor, was approved by the US Food and Drug Administration in 2015, improving the side effects associated with irreversible inhibitors such as selegiline and rasagiline[7]. However, there is still a limited number of hMAO-B inhibitors available. Therefore, the discovery of novel, highly selective, and reversible hMAO-B inhibitors with excellent blood−brain barrier permeability (BBB) is of therapeutic importance.

Natural products are a valuable resource for the discovery of novel enzyme inhibitors[8]. However, the dynamic range of secondary metabolites and numerous components of natural products have posed challenges for screening. In particular, the discovery of compounds in complex matrices relies on the separation of groups of active compounds. Currently, natural MAO-B inhibitors include alkaloids, flavonoids, coumarins, xanthones, anthraquinones, naphthoquinones, terpenes, terpenoids, phenols, and polyphenolic compounds[9]. Screening for MAO-B inhibitors from natural products mainly relies on bioassay-guided separation, which often suffers from frequent fractionation and long run times, high costs, and the loss of active substances[10]. To overcome these limitations, magnetic bead ligand fishing[11] and affinity ultrafiltration methods[12] have been proposed, enabling rapid separation of active compound groups and shortening the screening period to several months[13−15]. However, these methods also have limitations, including low throughput and the need for separate analysis after the identification of the active components. In 2011, Kool et al. proposed an at-line nano-fractionation approach, characterized by integrated sample separation, activity evaluation, and structure identification[16,17]. This approach offers advantages such as high throughput, high efficiency, and good reproducibility, making it widely used for high-throughput screening (HTS) of enzyme inhibitors from natural products. This method has been successfully applied to discover novel α-glucosidase[18], pancreatic lipase[19], trypsin[20], and neuraminidase inhibitors[21] from traditional Chinese medicines (TCMs) such as Ginkgo Biloba, green tea, *Cotinus coggygria* Scop. and Lonicerae Japonicae Flos, respectively. Therefore, the HTS of natural products targeting the mitochondrial membrane hMAO-B protein can provide inhibitors or pre cursor compounds for PD treatment.

In this study, a novel at-line nanofractionation platform was established for the HTS of hMAO-B inhibitors from natural products for the first time. The system stability, reproducibility as well as reliability were carefully optimized and evaluated. After conducting preliminary inhibitory screening of 29 Chinese medicines, Chuanxiong Rhizoma with good inhibitory activity was selected for hMAO-B inhibitors HTS. This screening allowed the rapid identification of organic acids, volatile oils, novel natural phthalides, and dimeric phthalides as potential hMAO-B inhibitors. Two new, potent, selective, and reversible hMAO-B inhibitors with good BBB permeability and neuroprotective effects comparable to commercial drugs rasagiline and safinamide were discovered.

2. Results and discussion

2.1. Establishment of hMAO-B inhibitors screening platform

The accurate identification of active substances from complex systems is a crucial factor in the screening process of bioassay systems, given the diverse structures and rich activities of compounds within such systems. Consequently, an at-line nano fractionation platform for screening hMAO-B inhibitors from complex systems was first established. This platform was validated using known commercial and natural MAO-B inhibitors.

The initial analysis was carried out with reported positive controls (rasagiline, calycosin, and isochlorogenic acid C) and negative controls (schisandrol A) (Fig. 1A and B). Subsequently, a mixed sample model was prepared to validate the effectiveness of the platform.

Meanwhile, due to the enzyme instability and the adsorption on the orifice plate, the enzymatic reaction lacks uniformity, leading to significant fluctuations in the system baseline of the bioactive spectrum. This, in turn, affects the accurate identification of inhibitors with low active peaks. Therefore, the reported nonionic surfactant Nonidet P-40 (NP-40) was used to improve the baseline noise on the hMAO-B screening system (Fig. 1C). Sequential elution of rasagiline, calycosin, isochlorogenic acid C, and schisandrol A was observed through RPLC, as depicted in Fig. 1C. Rasagiline and calycosin both displayed inhibitory activity, with the former having a correlatively smaller activity peak (Fig. 1C), which is surprising as it has a lower IC_{50} (0.1 *vs* 24 μmol/L, respectively). However, we believe this results from

the higher solubility of calycosin relative to rasagiline, indicating that this platform is better able to screen out bioactive substances with good solubility. The activity of the other positive controls demonstrated a positive correlation with the activity peak. Conversely, no activity peak was observed for the negative com pound, schisandrol A. Overall, these findings confirm the successful development of the screening system for hMAO-B in hibitors, enabling accurate and effective identification of such inhibitors within the mixed sample model.

To address the issue of baseline fluctuations, the added amounts of NP-40 (1%, 0.125%, 0.016%) were optimized based on preliminary experimental investigations (Fig. 1C). It was fou nd that 0.125% NP-40, which did not cause foaming or operational interference, significantly improved the baseline by reducing the adsorption of the enzyme on the plate. Therefore, it was deemed the most suitable NP-40 content for stabilizing the enzyme system. Fig. 1D shows the correlation between the size of the activity peak on the optimized screening platform and the sample concentration (50, 100, 200 μmol/L). As the concentration increased, the activity peaks of the positive controls exhibited a corresponding increase, indicating a positive correlation. Conversely, the negative compound did not generate any activity peak. This suggests a dose-effect relationship between the activity peak and the concentration of the active compound within the system. Furthermore, to enhance the accuracy of the high-throughput screening system, slight adjustments were made to the experimental protocol. In Fig. 1E, the positive control rasagiline (2 μmol/L) was represented in red, while the negative control DMSO (0.4%) was depicted in blue. The high-throughput screening factor (Z') was determined to be 0.72, and met the HTS requirement of $0.5 \leq Z' < 1$, indicating its suitability for further screening of hMAO-B inhibitors in complex systems[22].

2.2. *Screening of complex matrices to identify active extracts*

To identify Chinese medicines with the highest potential for hMAO-B inhibitory screening, the high-throughput fluorescent screening system was utilized to rapidly evaluate 29 Chinese medicines extracts commonly used in PD treatment, as reported in literature[23]. A heat map illustrates the inhibition of hMAO-B by these Chinese medicines extracts at concentrations of 1, 0.5, 0.125, 0.031, and 0.008 mg/mL, with the absence of an inhibitor serving as a blank control (Fig. 2A). The intensity of inhibition is represented by a color scale ranging from dark green to dark red, with increasing intensity indicating stronger inhibition. From the preliminary evaluation results, the top 12 extracts with the highest inhibitory activity were as follows: Chuanxiong Rhizoma > Glycyrrhizae Radix et Rhizoma > Epimedii Folium > Polygoni Cuspidati Rhizoma et Radix > Ramulus Uncariae cum Uncis > Nelumbinis Folium > Eucommiae Cortex > Siraitiae Fructus > Dendrobii Caulis > Artemisiae Argyi Folium > Lonicerae Japonicae Flos > Gastrodiae Rhizoma. Considering the relatively large concentration gradient used in the initial screening, it was challenging to accurately assess the inhibitory ability of a single medicinal material towards hMAO-B. Therefore, the top 12 extracts were further tested for their IC_{50} values against hMAO-B (Fig. 2B). It was observed that the order of inhibitory strength for some extracts (such as Glycyrrhizae Radix et Rhizoma and Polygoni Cuspidati

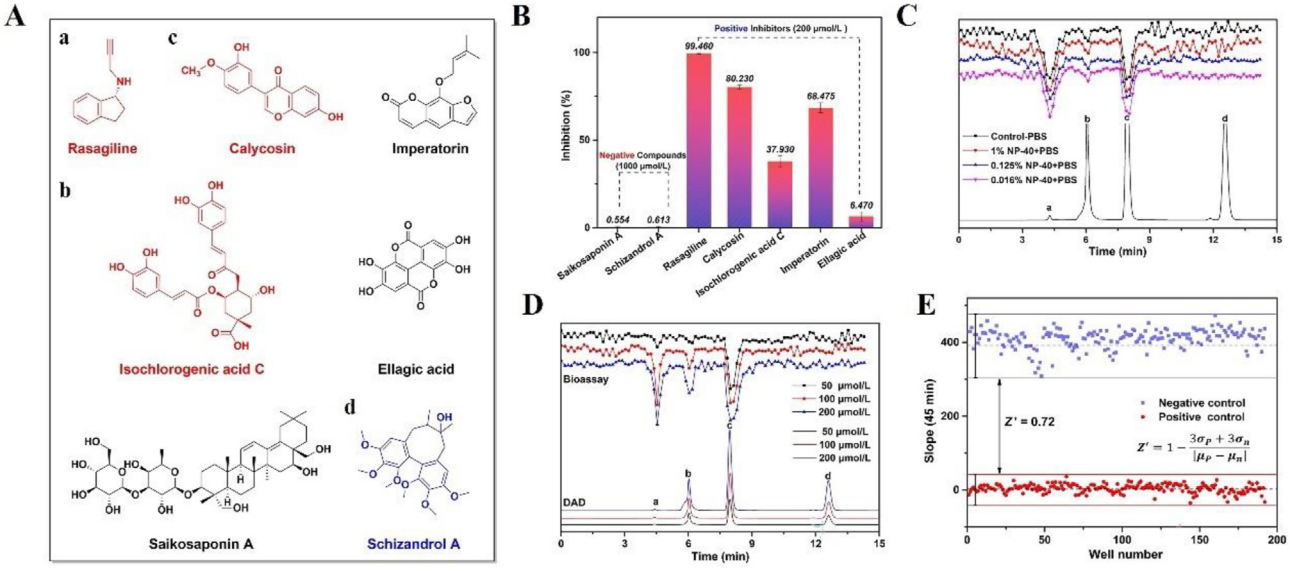

Figure 1 Development, optimization, and feasibility verification of screening platform for human monoamine oxidase B (hMAO-B) inhibitors. (A) Structures of MAO-B-related positive-negative compounds. (B) Evaluation of a screening library with negative and positive multi-structured standards. (C) Screening feasibility and baseline optimization of mixed standards at 100 μmol/L and (D) Investigation of the dose-response relationship of the screening system using different concentrations of mixed standards (a: rasagiline; b: isochlorogenic acid C; c: calycosin; d: schisandrol A). Sample: 100 μmol/L standards (rasagiline, isochlorogenic acid C, calycosin, and schizandrol A), 100% ethanol solution dissolved in 70% methanol, column: Zhongpu RD-C18 4.6 mm × 150 mm 5 μm 300 Å, mobile phase A: 0.1% Formic acid in Water, mobile phase B: 0.1% Formic acid in MeOH, isocratic elution: 73% B, flow rate: 0.5 mL/min, UV: 254 nm, temperature: 30 °C. (E) Data quality assessment of HTS assay in 384-well plates. σ_P and σ_n are the standard deviations of the positive control and negative control, respectively; μ_P and μ_n are the mean values of the positive control and negative control, respectively.

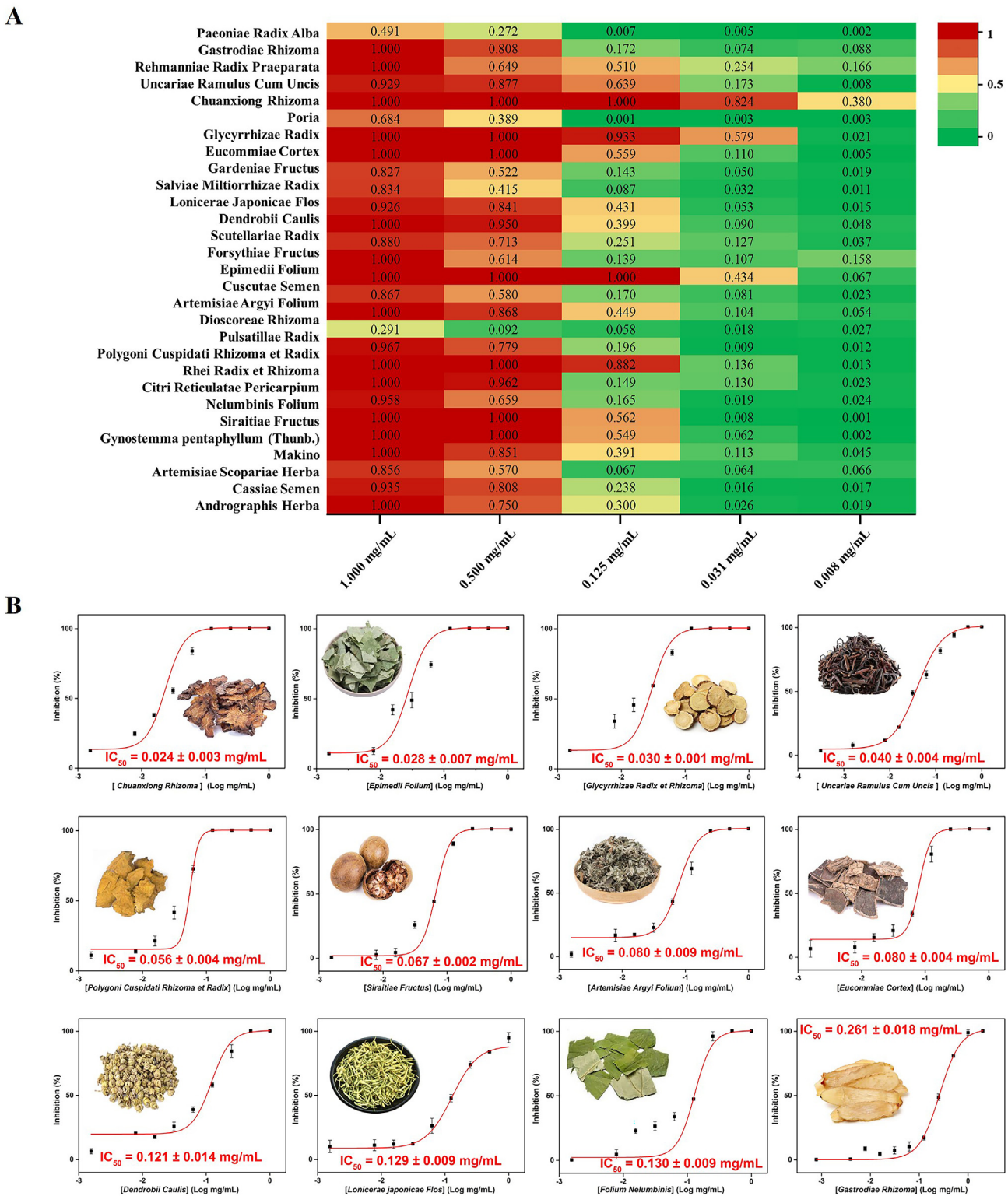

Figure 2 Evaluation of the inhibitory effect of several TCMs toward hMAO-B. (A) Inhibitory effect of 29 TCMs against hMAO-B. (B) IC_{50} values of the 12 most active TCMs towards hMAO-B.

Rhizoma et Radix) changed due to differences in solubility (Fig. 2A and B). The candidate natural product Chuanxiong Rhizoma was found to have the strongest inhibitory activity in both initial screening and half-inhibitory concentration determination results. Overall, the results of IC_{50} determinations provided a more reliable indication of hMAO-B inhibition by Chinese medicines.

A comprehensive analysis of factors such as inhibitory potency, reports of neurological diseases treatment, good water solubility of volatile components (volatile oils and phthalides), and phenolic acids was carried out. Chuanxiong Rhizoma was considered more suitable for the high-throughput screening of hMAO-B inhibitors than the other 11 candidates.

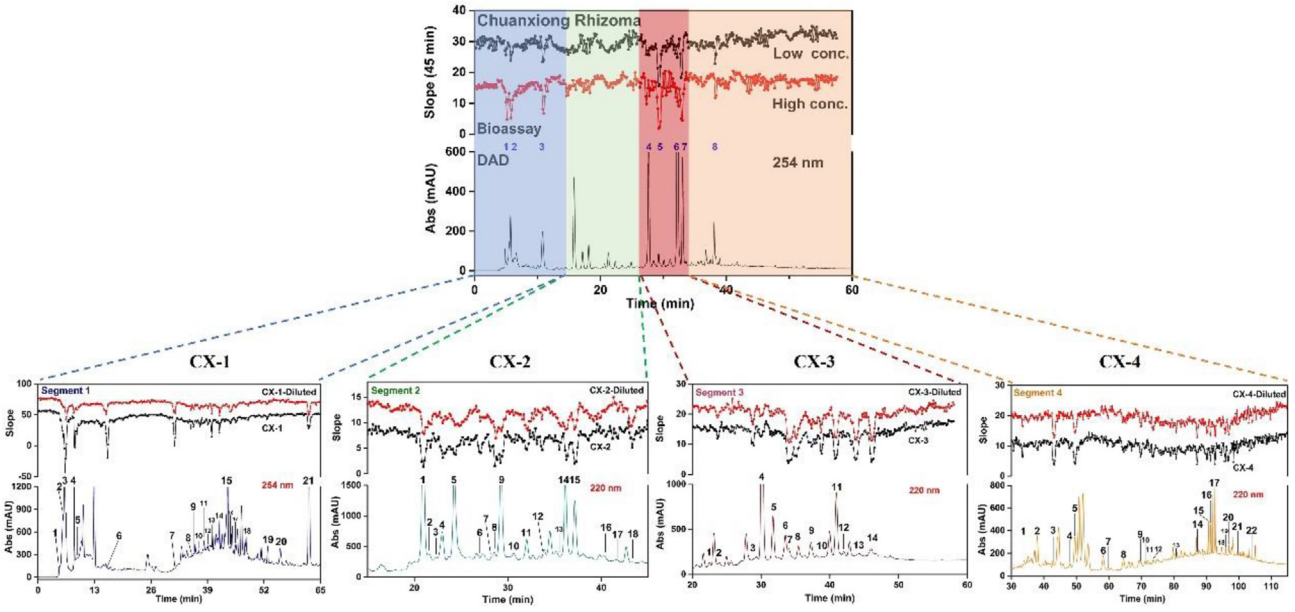

Figure 3 Inhibitory dose-response relationship activity spectrum of Chuanxiong Rhizoma and matching results of nearly 80 activity peaks after semi-preparative purification. HPLC gradient elution conditions for the four segments were as follows: Segment 1: RD-C18 column (3 μm), 0−15 min, 3%−4%, 15−30 min, 4%−15%, 30−50 min, 15%−20%, 30−50 min, 15%−20%, 50−70 min, 20%−25%, 70−85 min, 25%−30%, 85−95 min, 30%−100%, 95−115 min, 100%, 115−125 min, 100%−3% ACN; Segment 2: RD-C18 column (5 μm), 0−40 min, 45%−70%, 40−50 min, 70%−100%, 50−70 min, 100%, 70−75 min, 100%−45% MeOH; Segment 3: RD-C18 column (5 μm), 0−30 min, 55%−70%, 30−60 min, 70%−80%, 60−61 min, 80%−100%, 61−81 min, 100%, 81−85 min, 100%−55% MeOH; Segment 4: RD-C18 column (3 μm), 0−20 min, 65%−70%, 20−50 min, 70%, 50−90 min, 70%−100%, 90−120 min, 100%, 120−125 min, 100%−65% MeOH.

2.3. *Application of the developed platform to the high-throughput screening of hMAO-B inhibitors from Chuanxiong Rhizoma*

Traditionally, Chuanxiong Rhizoma is intended to promote blood circulation and *qi*, dispel *wind*, and relieve pain. It is often used in the palliative treatment of gynecological and cardiovascular diseases[24]. Chuanxiong's major chemical components, including volatile oils, alkaloids, phenolic acids, and phthalide lactones, display vasorelaxation, antioxidant properties, and neuroprotective effects, in both *in vitro* and *in vivo* studies[24]. Among them, ferulic acid (a representative compound of phenolic acids)[25] and ligustrazine[26] exert anticoagulant effects by inhibiting thrombin. At the same time, ferulic acid[27] and the phthalide compounds ligustilide[28] and ligustilide I[29] were reported to protect mitochondria and exert neuroprotective effects[30]. Recently, Feng's groups adopted the cytological profiling (CP) technique of hONS cells to discover chemical probes from 24 TCMs and preparations against PD[23]. In Chuanxiong Rhizoma, mainly phenolic acids and phthalide compounds were identified as active ingredients against PD[31]. However, it was noticed that their anti-PD and neuroprotective targets have not yet been elucidated.

Rapid and efficient high-throughput screening of Chuanxiong Rhizoma was conducted using the developed HTS platform for hMAO-B inhibitors. After optimizing the HPLC conditions, a preliminary screening was performed using 10 and 20 mg/mL Chuanxiong Rhizoma extract. As the compounds from Chuanxiong Rhizoma were sequentially eluted with methanol, the peaks with potential hMAO-B inhibitory activity were found to be correlated with the injected sample concentration. On a reverse phase chromatographic column, the major classes of compounds from Chuanxiong Rhizoma were eluted in the following order: organic acids, alkaloids, volatile oils, monophthalides, and diphthalides[32]. Eight activity peaks were initially identified from the samples of Chuanxiong Rhizoma. However, due to the complex composition and possible co-elution of compounds, the samples were divided into four fractions (Chuanxiong Rhizoma segments 1, 2, 3, 4) based on the distribution of activity peaks using a simplified semi-preparative LC method. After semi-preparative separation and optimization of HPLC conditions for each segment, the high-throughput screening of hMAO-B inhibitors was conducted for each segment of Chuanxiong Rhizoma. The semi-preparative purification made it possible to effectively enrich trace active in gredients in the Chuanxiong Rhizoma sample, resulting in the screening of nearly 80 peaks with potential hMAO-B inhibitory activity based on the dose-effect relationship. The activity peaks of segment 1 were mainly related to organic acids, those in segments 2 and 3 corresponded to phthalides, and those in segment 4 to phthalide dimers. Due to commercial availability, 14 representative standard compounds in Chuanxiong Rhizoma could be assigned to some of the activity peaks (Supporting Information Fig. S1).

2.4. *Potency and selectivity of identified hMAOs-B inhibitors*

To verify the effectiveness of this platform in HTS of hMAO-B inhibitors from crude Chuanxiong Rhizoma, we further tested the MAO inhibitory properties of identified representative compounds corresponding to activity peaks. The structures of these inhibitors are presented in Fig. 4, primarily consisting of organic acids and phthalides.

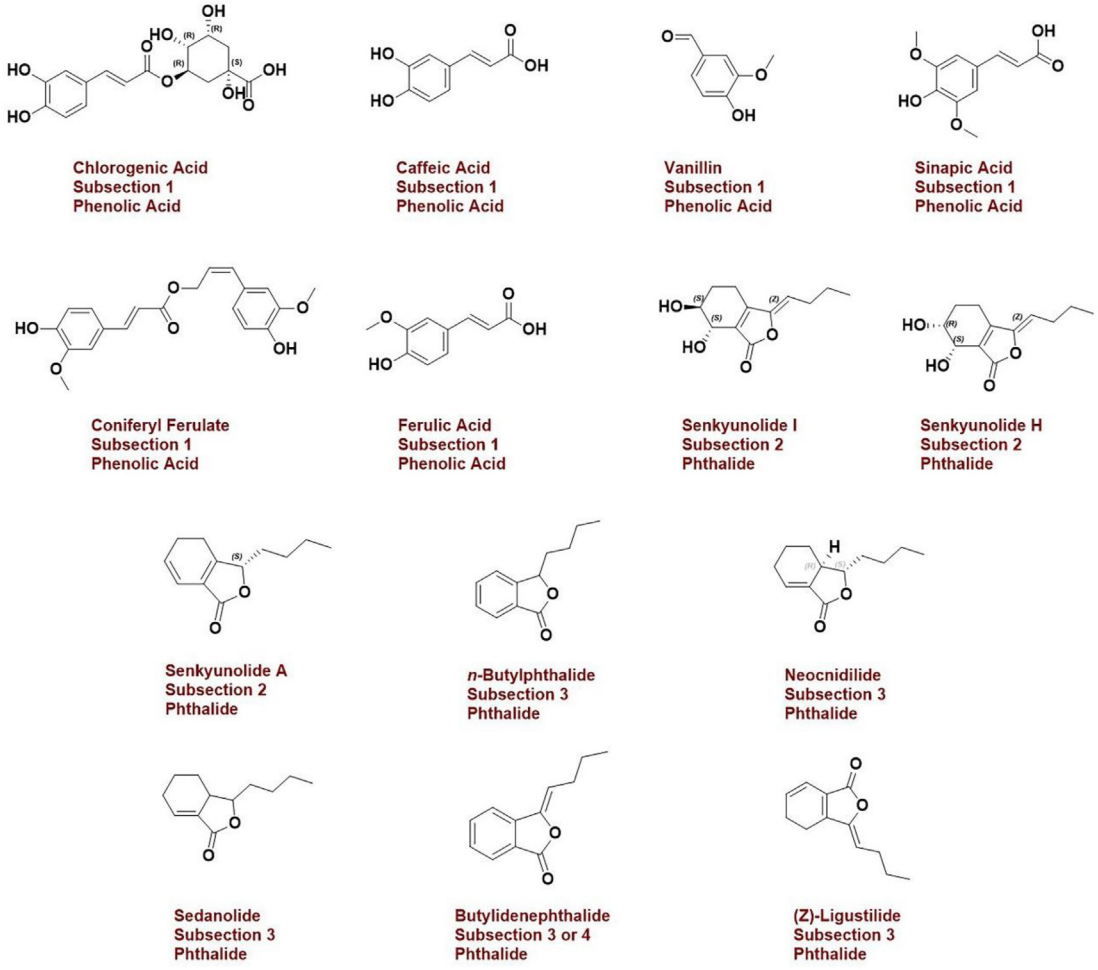

Figure 4 Structures of representative hMAO-B inhibitors identified in Chuanxiong Rhizoma.

The selectivity of hMAO-B inhibition relative to that of hMAO-A for these compounds is presented in Table 1. The inhibition selectivity of the known positive controls (rasagiline, safinamide, and toloxatone) is also reported in Table 1 and the results were consistent with those reported in literature[33].

Interestingly, phthalides with similar structures were found to exhibit different inhibitory activities against hMAO-B. For example, the characteristic components of Chuanxiong Rhizoma (senkyunolide H, senkyunolide I, and *z*-ligustilide) show slight inhibitory activity, *n*-butylphthalide has moderate activity, while senkyunolide A and butylidenephthalide possess good inhibitory activity, and sedanolide and neocnidilide have the highest activity. *n*-Butylphthalide is a classic first-line drug for the clinical treatment of ischemic stroke[34]. hMAO-A is one of the key indicators of ischemic stroke[35], and *n*-butylphthalide has also been reported to be used for neuroprotection and potential anti-PD properties[36]. As can be seen from Table 1, *n*-butylphthalide is indeed more effective in inhibiting hMAO-A, while its inhibitory activity against hMAO-B is more than 200 times lower than that of sedanolide and neocnidilide. It can be inferred that sedanolide and neocnidilide may have similar neuroprotective effects as *n*-butylphthalide. Phenolic acids inhibit hMAO-B in the sub micromolar concentration range, among which ferulic acid, chlorogenic acid[37], caffeic acid, and sinapic acid have all been reported to inhibit MAO-B in anti-PD extract[38]. Furthermore, vanillin and coniferyl ferulate are novel phenolic acid inhibitors of hMAO-B. These results successfully demonstrate that the proposed at-line nanofractionation platform enables rapid, efficient, and high-throughput screening of hMAO-B inhibitors in Chuanxiong Rhizoma. Phthalides and even dimerized phthalides were successfully identified as a novel class of natural hMAO-B inhibitors. Notably, sedanolide and neocnidilide exhibited remarkable inhibitory activity against hMAO-B, with sedanolide being equivalent to the positive control rasagiline in terms of inhibitory potency but surpassing it regarding selectivity for hMAO-B.

2.5. *Reversibility of hMAO-B inhibition*

A reversible inhibitor forms a complex with the enzyme, inhibits the interaction between enzyme and substrate[39], and reduces the oxidative deamination reaction rate of MAO-B, while irreversible inhibitors (known as covalent inhibitors) are often covalently bound to the enzyme active group to inactivate it. A study by Fowler and coworkers[40] showed that the turnover rate for MAO-B synthesis in human brain is close to 40 days. As a result, this may have safety issues and pharmacological side effects due to the persistent inhibition towards hMAO-B, such as immunogenicity of

Table 1 hMAO inhibitory potency and selectivity of identified compounds.

Compounds	Inhibition (IC_{50})[a]		SI[b]
	hMAO-B	hMAO-A	
(*Z*)-Ligustilide	633.346 ± 341.181	6.063 ± 0.985	0.009
Senkyunolide H	593.668 ± 55.172	107.921 ± 11.931	0.182
Senkyunolide I	302.342 ± 37.001	186.240 ± 8.010	0.616
n-Butylphthalide	112.552 ± 24.240	19.180 ± 3.759	0.170
Chlorogenic acid	69.634 ± 14.365	82.362 ± 14.569	1.183
Vanillin	45.695 ± 2.605	86.090 ± 15.313	1.884
Caffeic acid	33.093 ± 7.566	60.901 ± 5.847	1.840
Sinapic acid	32.783 ± 6.098	32.899 ± 5.705	1.004
Senkyunolide A	27.029 ± 9.316	47.573 ± 8.511	1.760
Ferulic acid	26.899 ± 3.528	35.828 ± 2.228	1.332
Butylidenephthalide	12.123 ± 6.480	96.986 ± 14.286	8.000
Coniferyl ferulate	2.029 ± 0.347	102.439 ± 1.331	50.487
Neocnidilide	0.494 ± 0.132	102.437 ± 13.108	207.362
Sedanolide	0.124 ± 0.033	80.067 ± 15.103	645.702
Rasagiline	0.114 ± 0.015	3.564 ± 0.386	31.263
Safinamide	0.006 ± 0.005	104.202 ± 34.732	17,367
Toloxatone	357.219 ± 22.843	1.438 ± 0.162	0.004

[a]Inhibition data are reported as IC_{50} (μmol/L); the standard error of the mean was always less than ± 5%.
[b]SI: selectivity index for the MAO-B isoform, equal to the ratio of IC_{50}(MAO-A)/IC_{50}(MAO-B).

enzyme-inhibitor complexes, adverse pharmacokinetic characteristics, inhomogeneity of tissue distribution, and longer duration of action and synthesis for recovering activity[41,42]. As reversible inhibitors such as safinamide are more effective and safer for the treatment of PD compared to irreversible inhibitors like rasagiline, the identification of reversible inhibitors is more promising.

Given their great potency and selectivity as hMAO-B inhibitors, the promising compounds sedanolide, neocnidilide, and coniferyl ferulate were selected for further investigation. The enzyme inhibition kinetics experiment with the advantage of reliable data points was adopted, as the most original reaction mechanism based on reversible or irreversible inhibition[43].

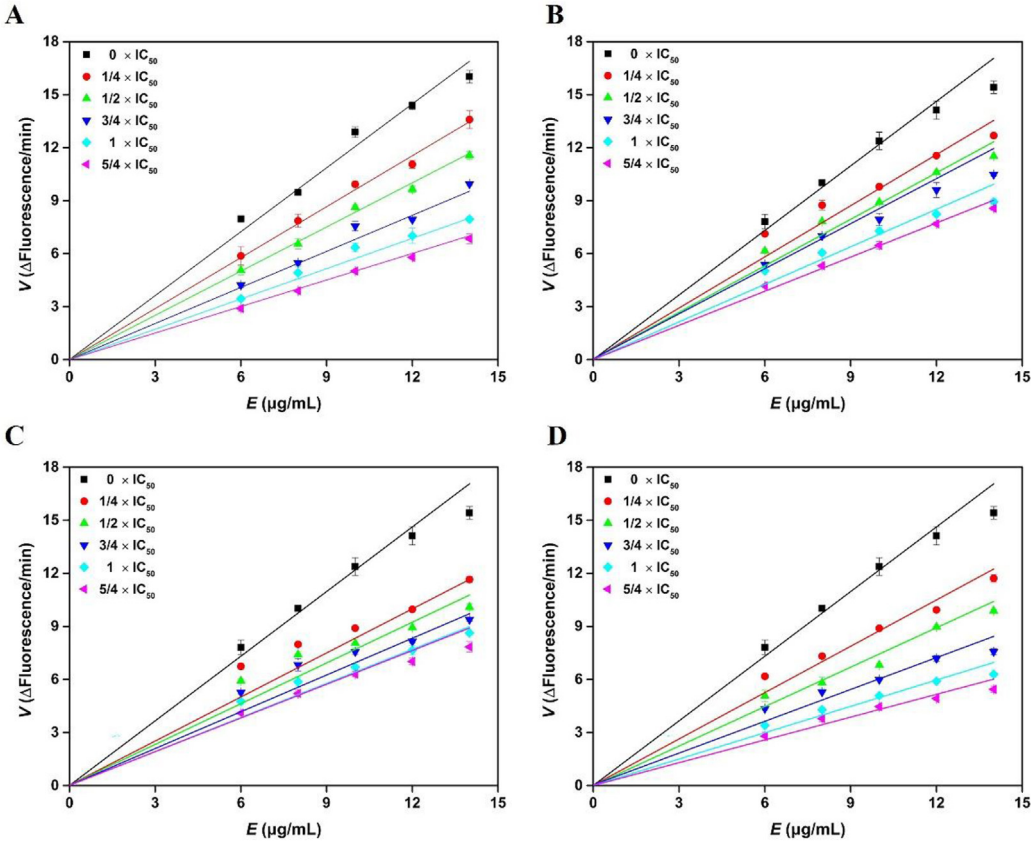

Figure 5 Plots of velocity *versus* hMAO-B concentration. (A) Safinamide, (B) Coniferyl ferulate, (C) Sedanolide, (D) Neocnidilide, kynuramine (KYN) concentration: 46 μmol/L.

Therefore, an enzyme inhibition experiment was performed to determine the inhibition reversibility of these compounds, with safinamide serving as a reversible reference compound. Briefly, plots of velocity (*V*) *versus* hMAO-B concentration were constructed using various concentrations of inhibitors to assess the reversibility of their hMAO-B inhibition (Fig. 5). The hMAO-B inhibitors tested were all shown to be reversible[44]. It is worth noting that two natural phthalides (sedanolide, and neocnidilide) were reversible inhibitors, which is consistent with the reported reversible hMAO-B inhibition of synthetic phthalides[45]. Thus, it can be speculated that most phthalide compounds are reversible inhibitors of hMAO-B. Studying phthalide compounds can help the precise development of reversible hMAO-B inhibitor drugs. These encouraging results provide motivation for drugability testing of the identified inhibitors.

2.6. *Evaluation of ADME properties and BBB permeability*

The BBB poses a significant challenge for the delivery of anti-PD and anti-AD agents to the central nervous system[46]. To assess the drug-likeness properties of the compounds, *in vitro* and *in vivo* absorption, distribution, metabolism, excretion, and toxicity (ADME/Tox) studies were carried out using Discovery Studio 2019. Additionally, a high-throughput assay of BBB permeability was performed using the IAM-HPLC method[47]. These results are shown in Supporting Information Table S2. The two classic anti-hMAO-B drugs rasagiline and safinamide and one first-line anti-ischemic stroke drug *n*-butylphthalide were employed as model prediction controls. Most compounds, except chlorogenic acid, were classified as soluble or moderately soluble, with highly predicted BBB permeability using Discovery Studio 2019, as shown in Table S2. These predictions were further supported by the results of BBB permeability obtained by IAM-HPLC. Notably, most phthalides exhibited higher water solubility and BBB permeability compared to organic acids. Among them, sedanolide and neocnidilide demonstrated superior solubility and BBB permeability compared to rasagiline and safinamide. The BBB permeability of neocnidilide was slightly higher than that of sedanolide. Both sedanolide and neocnidilide were identified as potent, selective, and BBB-permeant hMAO-B inhibitors.

2.7. *Neuroprotective effect of hMAO-B inhibitors on SH-SY5Y cells*

The above promising results demonstrating top inhibition potency and selectivity of sedanolide and neocnidilide against hMAO-B spurred further mechanistic studies and evaluation of their po tential as neuroprotective drugs targeting PD research. The SH-SY5Y neuroblastoma cell line, derived from humans and pos sessing catecholaminergic neural properties, is widely utilized in AD and PD research[48−50]. Therefore, the potential protective effects of sedanolide and neocnidilide against neurotoxin-induced

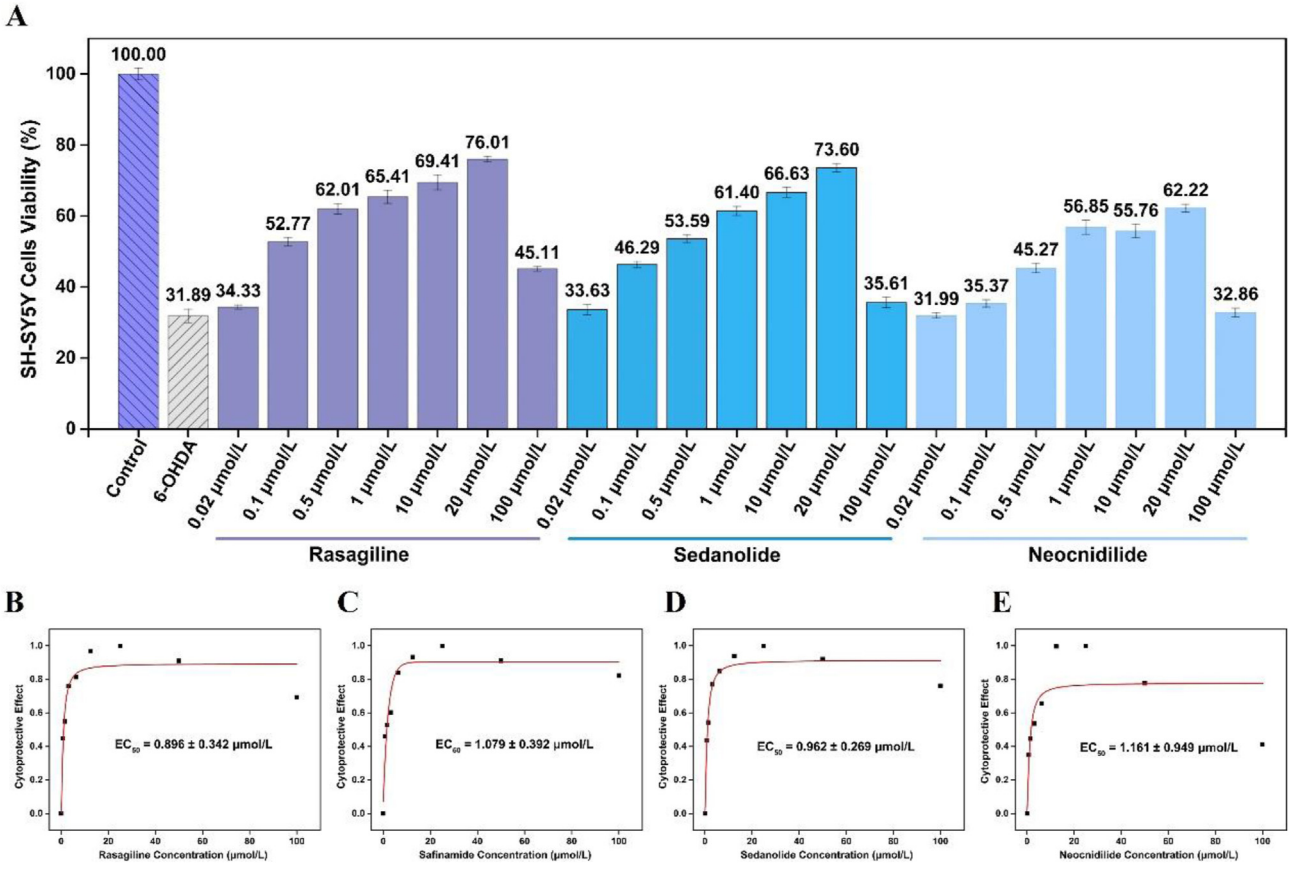

Figure 6 Neuroprotective effects of compounds on SH-SY5Y cells. Rasagiline and safinamide were used as reference compounds. Results were shown as percentages of cell viability. All data were the standard error of the mean of three independent experiments (compared to the 6-OHDA group). (A) Neuroprotective effects of MAO-B inhibitors against 6-OHDA-induced toxicity in SH-SY5Y cells. (B−E) Determination of the neuroprotective effect (EC_{50}) of MAO-B inhibitors on SH-SY5Y cells.

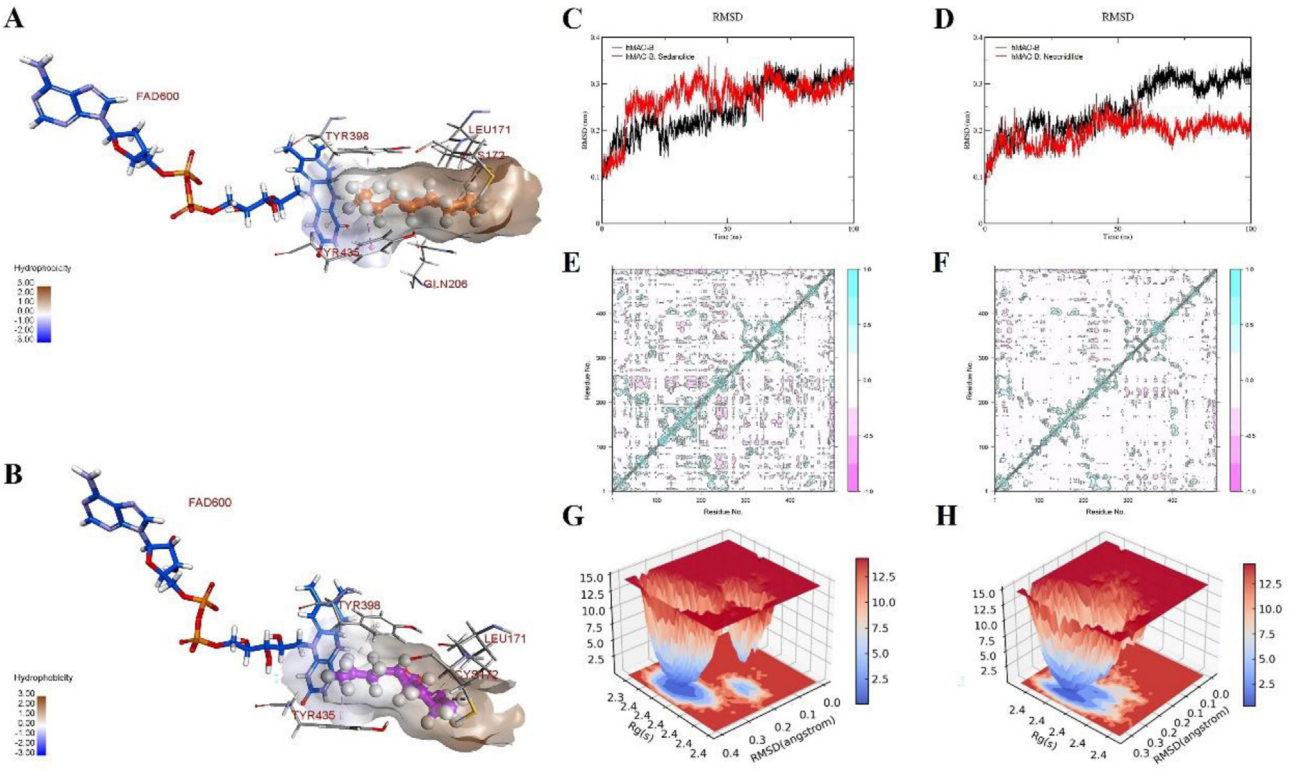

Figure 7 Molecular docking and molecular dynamics results for sedanolide and neocnidilide on hMAO-B (PDB: 2V5Z). 3D overview within the MAO-B active site over sedanolide (A) and neocnidilide (B). The root mean square deviations (RMSDs) of sedanolide (C) and neocnidilide (D) -hMAO B simulated structures. Covariance matrix diagrams of 100 ns binding to 2V5Z protein of sedanolide (E) and neocnidilide (F). Free-energy landscape diagrams of hMAO-B-sedanolide (G) and neocnidilide (H) clusters represented in 3D as a function of RMSD and radius of gyration (Rg).

damage were investigated in SH-SY5Y cells using the method described by Xie et al.[51] In this study, commercial drugs rasagiline and safinamide were employed as positive controls.

The bar chart in Fig. 6A illustrates that the cell viability rate of SH-SY5Y cells treated with 6-hydroxydopamine (6-OHDA, 200 μmol/L) significantly decreased to approximately 30% compared to the control group. However, when 6-OHDA-treated SH-SY5Y cells were incubated with increasing concentrations (0.02, 0.1, 0.5, 1, 10, 20 μmol/L) of the compounds, the cell survival rates gradually increased. Although slight cytotoxicity was observed at the high concentration of 100 μmol/L, the compounds still exhibited neuro protective effects similar to those observed with the reference com pound rasagiline under the same conditions. Furthermore, the third-generation reversible inhibitor safinamide was investigated for com parison of its half-maximal neuroprotective effect concentration (EC_{50}) with those of the other compounds. As shown in Fig. 6B−E, the results indicate the following order of neuroprotective effect: rasagiline (EC_{50} = 0.896 μmol/L) > sedanolide (EC_{50} = 0.962 μmol/L) > safinamide (EC_{50} = 1.079 μmol/L) > neocnidilide (EC_{50} = 1.161 μmol/L).

These results demonstrate that the neuroprotective capabilities of sedanolide and neocnidilide are similar to those of commercial drugs. It is important to emphasize that sedanolide exhibits cellular activity comparable to rasagiline and superior to safinamide, a first-in-class therapeutic targeting hMAO-B approved by the FDA. Particularly, it compared favorably to rasagiline in terms of inhibition reversibility and BBB permeability. The discovery of sedanolide as the most promising novel natural hMAO-B inhibitor through the use of the HTS platform is exciting, as it can be further developed and studied as a potential new drug for the treatment of neurodegenerative diseases.

2.8. Study of inhibition mechanism by molecular docking and molecular dynamics

To understand the molecular interaction of sedanolide and neocnidilide with hMAO-B, molecular docking and molecular dynamics (MD) were performed. The binding modes of inhibitors were investigated using the X-ray crystal structure of hMAO-B bound to safinamide [Protein Data Bank (PDB) code: 2V5Z][52] through Discovery Studio 2019. Molecular docking analysis was first applied to explore the bioactive conformations adopted within the binding pocket of hMAO-B enzyme. Table 2 shows that sedanolide presents a CD energy of −2.015 kJ/mol, while the CD energy for neocnidilide is −2.271 kJ/mol, which reflects a slight discrepancy with the reported inhibitory activities of the two compounds. The visualization of these results was performed with Discovery Studio 2019 (Fig. 7A and B). Fig. 7A shows the general 3D visualization of hMAO-B with the best pose of sedanolide within the active site, highlighting interactions with Gln 206, Leu 171, Cys 172, Tyr 435, Tyr 398 residues and the cofactor flavin adenine dinucleotide (FAD) 600. Correspondingly, Fig. 7B shows the 3D visualization of hMAO-B with neocnidilide, where interactions with the residues of Leu 171, Cys 172, Tyr 435, Tyr 398, and FAD 600 are formed. The above residues belong to the key amino acids in the hMAO-B active site[53,54]. Leu 171 is a neutral aliphatic amino

Table 2 Calculation of docking energy and binding free energy for sedanolide and neocnidilide with hMAO-B (PDB: 2V5Z).

Types	Name	Sedanolide	Neocnidilide
Molecular docking	CD ENERGY (kJ/mol)	−2.015	−2.271
	CD INTERACTION ENERGY (kJ/mol)	−36.288	−36.795
Molecular dynamics	ΔVDWAALS (kcal/mol)	−145.350	−150.390
	ΔE_{EL} (kcal/mol)	−112.550	−128.200
	ΔE_{GB} (kcal/mol)	125.500	138.090
	ΔE_{SURF} (kcal/mol)	−16.000	−15.900
	ΔG_{GAS} (kcal/mol)	−257.900	−278.590
	ΔG_{SOLV} (kcal/mol)	109.500	122.190
	ΔTOTAL (kcal/mol)	−148.400	−156.400

acid that forms the boundary of hMAO-B active site cavity, indicating that these compounds can bind to hMAO-B efficiently. In addition, Tyr 435, Tyr 398 and the cofactor FAD 600 are the keys to aromatic cage formation, recognizing substrate amino groups and their orientation. Unlike neocnidilide, sedanolide forms a hydrogen bond with Gln 206 (also an active residue of hMAO-B), which may explain the higher inhibitory effect of sedanolide compared to neocnidilide. However, the differences in docking energy needed to be further confirmed by molecular dynamics.

MD 100 ns simulation was carried out for hMAO-B complexes docked with the identified leads and the cocrystal inhibitor to understand the stability of binding. The results are summarized in Table 2 and Fig. 7. The root means square deviations (RMSDs) of the backbone and ligand were calculated against the initial structure of the protein-ligand complexes. The results for sedanolide and neocnidilide are presented in Fig. 7C and D, respectively.

During the 100 ns simulation, the neocnidilide−hMAO-B complex exhibited a lower RMSD value than the sedanolide−hMAO-B complex, which suggested that the neocnidilide−hMAO-B complex was more stable during the MD simulation. Here, the binding free energies of the two simulated complexes were computed to validate the affinities of the inhibitors predicted in docking studies. There was a good agreement between the binding free energies calculated using MD 100 ns trajectories and the molecular docking energies as shown in Table 2. Surprisingly, when we further visualized residue trajectories and total binding energies, we then discovered the details of sedanolide activity, superior to that of its isomer neocnidilide. The correlation and anticorrelation in residues of the movements in the complexes during an MD simulation are shown in Fig. 7E (sedanolide−hMAO-B complex) and Fig. 7F (neocnidilide−hMAO-B complex). In contrast with most residues in the neocnidilide−hMAO-B complex moving in the same direction, sedanolide moved more frequently and bound more closely to the 520 amino acid residues of hMAO-B. Thus, more pink areas appeared, indicating opposite movements. Also, this assertion was confirmed by the results of free energy landscapes of sedanolide (Fig. 7G) and neocnidilide (Fig. 7H). The areas shown in blue in Fig. 7G and H indicate the minimal energy areas and stability of the protein−ligand complexes. The highest stability of the complexes is represented by small and centralized blue areas and it also indicates that complexes were within the conformational cluster of hMAO-B. Moreover, narrow funnel-like projections reveal that the conformational cluster changes dynamically to the simulation time needed to achieve the least energy of the protein native structure[55]. Therefore, it can be seen that sedanolide leads to another funnel-shaped projection than neocnidilide from the 3D diagrams of the protein complexes formed by the two compounds. This clearly illustrates that the sedanolide−hMAO-B complex has more solitary local energy minima, thereby pointing toward two stable foldings for each of the protein−ligand complex systems. The above results can intuitively explain the difference in activity between sedanolide and neocnidilide.

3. Conclusions

In conclusion, we have successfully developed a high-throughput at-line nanofractionation screening platform for hMAO-B inhibitors, which demonstrated its efficiency in detecting active compounds in complex systems. It is worth emphasizing that we discovered two novel natural hMAO-B inhibitors from crude Chuanxiong Rhizoma, exhibiting druggability comparable to commercial drugs. In the initial screening, we evaluated 29 TCMs and identified 12 candidates with significant activity against hMAO-B for which IC_{50} values were determined. Among them, Chuanxiong Rhizoma, a classic Chinese medicine used in PD treatment, exhibited the best activity. By analyzing the activity chromatograms of Chuanxiong Rhizoma, we identified 75 chromatographic peaks with dose-dependent inhibitory activity against hMAO-B. Subsequently, 14 potentially active compounds were identified and selected through a combination of UPLC−Q-Orbitrap MS/MS data with LC and bioassay activity chromat ograms. Using the commercial drugs rasagiline and safinamide as controls, we investigated the inhibitory potency, selectivity, reversibility, and blood−brain permeability of these compounds. We further examined their pharmacokinetic and toxicological properties (ADMET), and inhibition reversibility, and elucidated the mechanisms of action and activity differences on hMAO-B through molecular docking and molecular dynamics experiments. Among these compounds, sedanolide and neocnidilide exhibited excellent performance and were identified as promising drug candidates. Notably, in SH-SY5Y cell experiments, sedanolide and neocnidilide demonstrated neuroprotective effects com parable to those of rasagiline and safinamide, with sedanolide showing superior efficacy. Moreover, molecular docking and molecular dynamics data could be used to explain their inhibition mechanisms and activity differences towards hMAO-B. Both sedanolide and neocnidilide were identified as next-generation drug candidates with excellent drug-like properties and superior pharmacological profiles for the treatment of PD. These exciting possibilities should be examined in future investigations.

4. Experimental

4.1. Chemicals and materials

Human recombinant MAO-A (hMAO-A) and MAO-B (hMAO-B) enzymes prepared from insect cells, kynuramine dihydrobromide

(KYN; 98%), 4-hydroxy quinoline (98%) and toloxatone (98%) were obtained from Sigma−Aldrich (St. Louis, MO, USA). Safinamide (>98%) was from TCL (Tokyo Chemical Industry Co., Ltd., Tokyo, Japan). HPLC-grade methanol (MeOH) and acetonitrile (ACN) were purchased from Merck (Darmstadt, Germany). Sodium phosphate dibasic (Na_2HPO_4; 99%), potassium phosphate monobasic (KH_2PO_4; 99%), potassium chloride (KCl; 99%), sodium chloride (NaCl; 99%), formic acid (FA; 98%), dimethyl sulfoxide (DMSO; 99%), schisandrol A (99%) were bought from Aladdin Chemistry (Shanghai, China). Rasagiline (98%) and isochlorogenic acid C (98%) were from Macklin (Shanghai, China). Calycosin (98%), and sedanolide (98%) were obtained from Sichuan Weikeqi Biological Technology Co., Ltd. (Sichuan, China). Neocnidilide (98%) was from ChemFaces (Wuhan, China). Other chemicals were purchased from standard sources and were of the highest quality available. All chemicals were of HPLC grade and used without further purification. Herbal medicines including Gastrodiae Rhizoma and Uncariae Ramulus Cum Uncis were provided by Kangmei Pharmaceutical Co., Ltd. (Guangdong, China). Other herbal medicines such as Chuanxiong Rhizoma and Rehmanniae Radix Praeparata were purchased from Tongrentang Chinese Medicine (Beijing, China). The remaining Chinese herbal medicines in the form of lyophilized aqueous extract powder were all manufactured by the Yifang Pharmaceutical Co., Ltd. (Guangdong, China). Cell counting kit-8 (CCK-8) was purchased from MedChemExpress company (HY-K0301, Shanghai, China). Dulbecco's modified Eagle's medium (DMEM), Nutrient Mixture Ham's F-12 (DMEM/F12 1:1) medium, fetal bovine serum (FBS) and phosphate-buffered saline (PBS) were bought from Gibco (Carlsbad, CA, USA). 6-Hydroxydopamine hydrochloride (6-OHDA) was obtained from Sigma−Aldrich (St. Louis, MO, USA).

384-well plates (3573) were supplied by Corning (NY, USA). De-ionized water was purified by a Milli-Q water purification system (Millipore, Molsheim, France). Centrifugation was carried out in a refrigerated centrifuge Model Allegra X-30R (Beckman Coulter, Brea, CA, USA). The bioassay test was carried out using a Multidrop 384 reagent dispenser (Thermo Fisher Scientific, Waltham, MA, USA), then monitored with a Synergy 2 monochromator-based microplate reader (BioTek, Winooski, VT, USA). Samples and well plates containing samples were dried in a vacuum oven from Shanghai Xiaohan Industrial Development Co., Ltd. (XHDZF-6050, Shanghai, China).

4.2. *Preparation of traditional Chinese medicine extracts*

Dried Chinese herbal medicines (50 g) were milled (550 W, over 50 mesh size) by a multi-functional pulverizer (BJ-150, Baijie, Shanghai, China). Then, they were sonicated three times (40 kHz, 250 W) in 500 mL 70% ethanol aqueous solution for 30 min at 30 °C, using an SB-5200 DTD ultrasonicator (Scientz, Ningbo, China). After filtration, the 70% ethanol extracts were dried in a Heidolph rotary evaporator (Hei-VAP, Heidolph, Schwabach, Germany), collected and stored at −20 °C before use.

4.3. *hMAO-B bioassay*

The potential effects of compounds on human MAO activity were investigated according to a previously described fluorescence method based on kynuramine oxidation with slight adjustments[56]. Rasagiline, safinamide, and toloxatone were used as reference compounds[57]. The experiment consisted of measuring the fluorescence of 4-hydroxy quinoline produced from kynuramine dihydrobromide, using the oxidative deamination properties of recombinant human MAOs.

25 μL hMAO-B enzyme solution (8 μg/mL) and 25 μL KYN solution (46 μmol/L) containing various concentrations of the test compound in DMSO (less than 2%) constituted a 50 μL final volume of hMAO-B fluorescence kinetic reaction system in aqueous phosphate buffered saline (PBS, 100 mmol/L, pH 7.4). On the other hand, hMAO-A enzyme (5 μg/mL) activity detection system was adjusted to be consistent with the catalytic rate of hMAO-B.

Usually, the inhibitor-containing substrate and enzyme solutions were respectively dispensed into a 384 black microplate using an electronic multi-channel pipette, and then centrifuged at 2000 rpm for 3 min to mix them well. Afterwards, the kinetics of the enzymatic reaction were quantitatively monitored using a microplate fluorescence reader at 37 °C for 8 cycles at excitation and emission wavelengths of 315 and 370 nm, respectively. The inhibitory rate was calculated as Eq. (1):

$$\text{Inhibition}\,(\%) = \frac{S_0 - S_i}{S_0 - S_b} \times 100 \tag{1}$$

where S_i and S_0 are the slopes of fluorescence growth in the presence and absence of inhibitor, S_b is the control slope determined in the absence of enzyme and inhibitor. Data were shown as a mean ± SD of three independent experiments and the eventual IC_{50} values were calculated using Origin 9.0 software (Origin Lab, Northampton, MA, USA). According to preliminary experimental investigation, 0.125% of the non-ionic surfactant NP-40 was added separately to the detection buffer system to reduce baseline fluctuations.

4.4. *High-throughput platform for screening hMAO-B inhibitors*

The complete at-line nanofractionation screening platform for hMAO-B inhibitors included HPLC separation and activity detection.

Samples (20 μL) were analyzed using HPLC equipment (Shimadzu LC-20AT, Tokyo, Japan) fitted with a SIL 20A autosampler, a CTO-20A oven, an LC-20AT pump system with a flow rate of 0.5 mL/min and an SPD-M20A photodiode array detector with a class LC10 chromatography workstation. The column temperature was set at 30 °C. RD-C18 columns (250 mm × 4.6 mm, 5 μm or 3 μm) equipped with an RD-C18 guard column (4.0 mm × 3.0 mm i.d.) from Zhongpu Science (Guangzhou, China) were used for all separations. Mobile phase A consisted of 0.1% FA in H_2O, while mobile phase B was 0.1% FA in MeOH or ACN. The gradient programs varied from one sample to another and can be found in the legend of Fig. 3. All sample solutions were filtered through a 0.22 μm membrane filter before injection into the chromatographic system.

The high-resolution hMAO-B bioassay was performed according to the reported standard literature protocols[18] with slight adjustments. After HPLC separation, the eluent was split in a 1:1 ratio. The other eluent portion was directed to LC−MS/MS.

LC−MS/MS analyses were performed using a Vanquish ultra-high performance liquid chromatography system coupled to an Orbitrap Exploris 120 mass spectrometer (Orbitrap MS, Thermo Fisher Scientific, Waltham, MA, USA). MS/MS spectra were acquired in data-dependent acquisition (DDA) mode under the

control of the acquisition software (Xcalibur 4.0.27, Thermo Fisher Scientific, Waltham, MA, USA). The injection volume was 2 μL, the calibration of mass accuracy was performed with leucine enkephalin as an internal standard, and positive and negative ions were scanned separately. The ESI source parameters were set as follows: sheath gas flow rate: 50 Arb; aux gas flow rate: 10 Arb; capillary temperature: 320 °C; evaporator temperature: 400 °C; full MS resolution: 60,000; MS/MS resolution: 15,000; collision energy: 20/50/80 in HCD mode; spray voltage: 3.5 kV (positive) or −3.0 kV (negative), respectively.

4.5. *Semi-preparative purification of Chuanxiong Rhizoma extracts*

The four fractions of Chuanxiong Rhizoma extract were purified using a semi-preparative Agilent 1200 Series chromatograph (Agilent Technologies, California, USA) coupled to a variable-wavelength ultraviolet detector (Agilent 1200 Series, G1314B). Separations were performed on an RD-C18 column (250 mm × 10 mm, 5 μm) equipped with an RD-C18 pre-column (4.0 mm × 3.0 mm i.d.) from Zhongpu Science (Guangzhou, China). A 50 mg/mL sample solution in 70% methanol was analyzed using an injection volume of 500 μL−1 mL, a flow rate of 3 mL/min, and a detection wavelength of 254 and 220 nm. Mobile phases were consistent with the high-resolution activity chromatogram. Gradient elution was carried out as follows: 0−30 min, 40%−80%, 30−45 min, 80%−90%, 45−55 min, 90%−100%, 55−80 min, 100% MeOH.

According to the distribution area of active peaks and the component distribution in each period, some post-column effluents from different periods were collected. For segment 1 the period was 0−15 min, for segment 2, 16−25 min, for segment 3, 26−40 min and for segment 4, 41−80 min. Later, the segments were dried by rotary evaporation at 45 °C to obtain the crude extracts, which were sealed and stored in a −20 °C refrigerator.

4.6. *Analysis of mass spectrometry data*

According to mass spectrometry information data retrieved from Chuanxiong Rhizoma, the database of compounds in Chuanxiong Rhizoma was elaborated by referring to literature[58−60]. It was then combined with a high-resolution mass spectrometry database of traditional Chinese medicine components (OTCML), mzCloud, ChemSpider online mass spectrometry database, mzVault 2.0, Masslist mass spectrometry database, Compound Discoverer 3.3 software, and Mass Frontier 8.0 software (Thermo Fisher Scien tific, Waltham, MA, USA), which provided fragmentation fragments for comparison, and elucidation of the structure of poten tially active compounds based on secondary fragment ions (Supporting Information Table S1).

4.7. *Reversibility of hMAO-B inhibition*

The inhibition reversibility and type of hMAO-B inhibition induced by sedanolide and neocnidilide were evaluated by kinetic analysis. The inhibitory models were calculated using the Lineweaver-Burk equation. A series of inhibitors solutions (0.25 × IC_{50}, 0.5 × IC_{50}, 0.75 × IC_{50}, 1 × IC_{50}, 1.25 × IC_{50}) were mixed with different concentrations of hMAO-B (6, 8, 10, 12, 14 μg/mL) with a fixed KYN concentration (46 μmol/L), to test inhibition reversibility.

4.8. *Blood−brain barrier permeability*

ADME/Tox properties were predicted using the Discovery Studio 2019 program client version (Neotrident Technology Ltd., Beijing, China), with an emphasis on compound solubility, BBB permeability, and small intestinal absorption[61]. In addition, blood−brain barrier penetration was further verified by experiments using immobilized artificial membrane (IAM) chromatography[47]. IAM-based chromatographic analysis was performed on an Agilent 1200s system (Santa Clara, CA, USA), with an IAM.PC.DD column (4.6 mm × 10 cm, 5 μm, 300 Å) purchased from Regis Technologies (Morton Grove, IL, USA). The mobile phase was a mixture of acetonitrile and Dulbecco's phosphate-buffered saline (DPBS) (20: 80, *v*/*v*) with pH adjusted to 7.0 using HCl. The flow rate of the mobile phase was set at 0.5 mL/min, the temperature at 30 °C, and the ultraviolet absorption wavelength at 210 nm.

4.9. *Cell viability assay*

The viability of human neuroblastoma (SH-SY5Y) cells was determined by CCK-8 assay according to a previously described method[51]. SH-SY5Y cells were from American Type Culture Collection (ATCC, Manassas, VA, USA) and maintained in DMEM/F12 medium containing 10% (*v*/*v*) FBS and 1% penicillin/streptomycin in a humidified atmosphere of 5% CO_2 and 95% air at 37 °C. Cells were seeded in a 96-well plate at 1 × 10^4 cells/well for 24 h at 37 °C with 5% CO_2 and treated with 200 μmol/L 6-OHDA for 16 h. The culture medium was removed and the cells were then treated with different concentrations of inhibitors for 4 h before stimulation with 10 μL of CCK-8 solution, with rasagiline and safinamide as positive controls. Absorbance was measured at 450 nm with a microplate reader. Control cells treated with DMSO alone were regarded as having 100% viability. Each compound solution was diluted in a cell medium to reach the desired concentration. The concentration of DMSO in each well was always lower than 0.1%. All results were presented as the mean ± SD of three independent experiments. EC_{50} values for neuroprotection represent 50% effect exerted by compounds in cells and were calculated from a logistic dose-response curve using Origin 9.0 software.

4.10. *Molecular docking*

The docking analysis was carried out using a Discovery Studio 2019 program client version (Neotrident Technology Ltd., Beijing, China)[62]. The X-ray crystal structure of hMAO-B complexed with safinamide with a resolution of 1.60 Å was obtained from the RCSB Protein Data Bank (https://www.rcsb.org/) (PDB ID: 2V5Z)[63]. The ligand and water molecules were removed from the crystal structure, and then hydrogen atoms were added. Since hMAO-B is a homodimer, only the A chain and FAD 600 were retained. The structures of the active compounds were obtained from the PubChem database (https://pubchem.ncbi.nlm.nih.gov/) and the SciFinder database (https://scifinder-n.cas.org/), and then energy minimization was conducted. For semi-flexible docking, the active site according to the safinamide-protein binding pocket was set as (51.8861, 156.453, 28.5591, 10). The absolute value of the molecular docking score represents the binding force between an active compound and the therapeutic target. The higher the score, the stronger the binding force.

4.11. Molecular dynamics

Parameterized molecular dynamics of hMAO-B with FAD 600 and active compounds were carried out using the AMBER FF99SB force field[54]. The corresponding.mol2 and.pdb files were generated based on three digits of precision for atomic coordinates over optimal conformation of inhibitors with hMAO-B. Gauss View 5.0 was adopted to detect the structural integrity of the protein, small molecules, and FAD and completely convert them to.gif format. Then, a p B3LYP/6-31G* opt freq operation code was added to the.gif format file, which was used to calculate the precise charge of the protein and compounds. Subsequently, Gaussian 16 software was implemented to run a charge calculation of.gif, convert the calculation result to.fchk format, start Multiwfn, and calculate the standard RESP charge, to generate a.chg file. The.mol2 files of hMAO-B and compounds were then imported into Sobtop 1.0 (dev3) software (Beijing, China) for corresponding topology structures, and.gro, .top, and.itp files for GROMACS calculations were generated. Charges in.itp were replaced with charges in.chg. Later, based on the AMBER99SB force field and TIP3P water box model (with 10 Å buffer), the hMAO-B−compound and hMAO-B−FAD complexes, the atomic coordinate axis information of hMAO-B, FAD, and compounds were respectively constructed and integrated into a total topology file, followed by 100 ns molecular dynamics operation.

Docked complexes of protein, FAD, and compound were limited, and solvated, and Na^+ and Cl^- ions were added for charge neutralization. Afterward, energy minimization consisted of 1000 cycles of steepest descent. The first simulation was a Brownian dynamics run for 200 ps at 310.15 K in a canonical ensemble (NVT) ensemble (1 atm). Further, MD simulation for 500 ps was performed in a constant pressure-constant temperature (NPT) ensemble (310.15 K, 1 atm). The abovementioned equilibration was followed by a 100 ns simulation with a 2 fs integration time step, during which 1000 trajectories were saved. GROMACS, GMX MMPBSA, VMD, and R languages were used to calculate and visualize results such as RMSD, root mean square fluctuation (RMSF), binding free energy, energy decomposition of binding free energy, hydrogen bond changes, free energy surface plots, and amino acid residue covariance plots.

Acknowledgments

This work was supported by grants from the National Natural Science Foundation of China (82073806, 82304437, 82204342, 82373835, 82173781). The China Postdoctoral Science Foundation (2022M721355, China), and the Fundamental Research Funds for the Central Universities (21623343, China).

Author contributions

Zhengjin Jiang and Tingting Zhang conceived the research. Yu Fan designed the research, performed the experiments, analyzed data, and wrote the manuscript. Jincai Wang and Jingyi Jian built an at-line nanofractionation platform, assisted in experiments, and helped with manuscript revision. Yalei Wen performed cell-based assays. Jiahao Li directed the molecular docking and assisted in carrying out the initial part of molecular dynamics. Hao Tian provided conceptual advice and contributed to the analysis of the data. Jacques Crommen improved the manuscript. Zhengjin Jiang, Tingting Zhang, and Wei Bi directed and supervised the research. All authors reviewed the results and approved the final version of the manuscript.

Conflicts of interest

The authors declare no competing interests.

Appendix A. Supporting information

Supporting data to this article can be found online at https://doi.org/10.1016/j.apsb.2024.01.020.

References

1. Bloem BR, Okun MS, Klein C. Parkinson's disease. *The Lancet* 2021;**397**:2284−303.
2. Group PMC. Long-term effectiveness of dopamine agonists and monoamine oxidase B inhibitors compared with levodopa as initial treatment for Parkinson's disease (PD MED): a large, open-label, pragmatic randomised trial. *The Lancet* 2014;**384**:1196−205.
3. Yap SY, Frias B, Wren MC, Schöll M, Fox NC, Årstad E, et al. Discriminatory ability of next-generation tau PET tracers for Alzheimer's disease. *Brain* 2021;**144**:2284−90.
4. Binda C, Newton-Vinson P, Hubálek F, Edmondson DE, Mattevi A. Structure of human monoamine oxidase B, a drug target for the treatment of neurological disorders. *Nat Struct Biol* 2002;**9**:22−6.
5. Tsuboi T, Satake Y, Hiraga K, Yokoi K, Hattori M, Suzuki M, et al. Effects of MAO-B inhibitors on non-motor symptoms and quality of life in Parkinson's disease: a systematic review. *NPJ Parkinson's Dis* 2022;**8**:1−21.
6. Voelker R. New addition to Parkinson therapy. *JAMA* 2017;**317**:1716.
7. Schapira AHV, Fox SH, Hauser RA, Jankovic J, Jost WH, Kenney C, et al. Assessment of safety and efficacy of safinamide as a levodopa adjunct in patients with Parkinson disease and motor fluctuations: a randomized clinical trial. *JAMA Neurology* 2017;**74**:216−24.
8. Atanasov AG, Zotchev SB, Dirsch VM, Supuran CT. Natural products in drug discovery: advances and opportunities. *Nat Rev Drug Discovery* 2021;**20**:200−16.
9. Chaurasiya N, Leon F, Muhammad I, Tekwani B. Natural products inhibitors of monoamine oxidases-potential new drug leads for neuroprotection, neurological disorders, and neuroblastoma. *Molecules* 2022;**27**:4297.
10. Banerjee C, Nandy S, Chakraborty J, Kumar D. Myricitrin-a flavonoid isolated from the Indian olive tree (*Elaeocarpus floribundus*)−inhibits monoamine oxidase in the brain and elevates striatal dopamine levels: therapeutic implications against Parkinson's disease. *Food Funct* 2022;**13**:6545−59.
11. Moaddel R, Marszałł MP, Bighi F, Yang Q, Duan X, Wainer IW. Automated ligand fishing using human serum albumin-coated magnetic beads. *Anal Chem* 2007;**79**:5414−7.
12. He Y, Wang YM, Zhang X, Zheng Z, Liu S, Xing JP, et al. Chemical characterization of small-molecule inhibitors of monoamine oxidase B synthesized from the *Acanthopanax senticosus* root with affinity ultrafiltration mass spectrometry. *Rapid Commun Mass Spectrom* 2020;**34**:e8694.
13. Hu YK, Liu YM, Bai XL, Ma C, Liao X. Screening of monoamine oxidase B inhibitors from *Fragaria nubicola* by ligand fishing and their neuroprotective effects. *J Agric Food Chem* 2023;**71**:512−21.
14. Qi XW, Liu YM, Hu YK, Yuan H, Ayeni EA, Liao X. Ligand fishing based on tubular microchannel modified with monoamine oxidase B for screening of the enzyme's inhibitors from *Crocus sativus* and *Edgeworthia gardneri*. *J Sep Sci* 2022;**45**:2394−405.
15. Jiang XL, Yuan YC, Chen LB, Liu YM, Xiao MW, Hu YD, et al. Monoamine oxidase B immobilized on magnetic nanoparticles for screening of the enzyme's inhibitors from herbal extracts. *Microchem J* 2019;**146**:1181−9.

16. Kool J, De Kloe G, Denker AD, Van Altena K, Smoluch M, Van Iperen D, et al. Nanofractionation spotter technology for rapid contactless and high-resolution deposition of LC eluent for further off-line analysis. *Anal Chem* 2011;**83**:125−32.
17. Xie CF, Slagboom J, Albulescu LO, Somsen GW, Vonk FJ, Casewell NR, et al. Neutralising effects of small molecule toxin inhibitors on nanofractionated coagulopathic Crotalinae snake venoms. *Acta Pharm Sin B* 2020;**10**:1835−45.
18. Liu RJ, Kool J, Jian JY, Wang JC, Zhao XL, Jiang ZJ, et al. Rapid screening α-glucosidase inhibitors from natural products by at-line nanofractionation with parallel Mass spectrometry and bioactivity assessment. *J Chromatogr A* 2021;**1635**:461740.
19. Jian JY, Yuan JM, Fan Y, Wang JC, Zhang TT, Kool J, et al. High-resolution bioassay profiling with complemented sensitivity and resolution for pancreatic lipase inhibitor screening. *Molecules* 2022;**27**:6923.
20. Wang JC, Huang XL, Mei J, Chen XW, Ma R, Li GW, et al. Screening of trypsin inhibitors in *Cotinus coggygria* Scop. extract using at-line nanofractionation coupled with semi-preparative reverse-phase liquid chromatography. *J Chromatogr A* 2023;**1691**:463817.
21. Chen ZX, Wang JC, Yuan JM, Wang Z, Tu ZC, Crommen J, et al. Rapid screening of neuraminidase inhibitors using an at-line nanofractionation platform involving parallel oseltamivir-sensitive/resistant neuraminidase bioassays. *J Chromatogr A* 2023;**1687**:463693.
22. Zhang JH, Chung TD, Oldenburg KR. A simple statistical parameter for use in evaluation and validation of high throughput screening assays. *J Biomol Screen* 1999;**4**:67−73.
23. Wang C, Yang XZ, Mellick GD, Feng YJ. Meeting the challenge: using cytological profiling to discover chemical probes from traditional Chinese medicines against Parkinson's disease. *ACS Chem Neurosci* 2016;**7**:1628−34.
24. Ran X, Ma L, Peng C, Zhang H, Qin LP. Ligusticum chuanxiong Hort: a review of chemistry and pharmacology. *Pharm Biol* 2011;**49**:1180−9.
25. Huang CC, Zhao Y, Huang SY, Li L, Yuan ZY, Xu GM. Screening of anti-thrombin active components from Ligusticum chuanxiong by affinity-ultrafiltration coupled with HPLC−Q-Orbitrap-MSn. *Phytochem Anal* 2023;**34**:443−52.
26. Zhang YF, Ma C, He LF, Liao L, Guo CC, Wang C, et al. Tetramethylpyrazine protects endothelial injury and antithrombosis *via* antioxidant and antiapoptosis in HUVECs and zebrafish. *Oxid Med Cell Longev* 2022;**2022**:e2232365.
27. Barone E, Calabrese V, Mancuso C. Ferulic acid and its therapeutic potential as a hormetin for age-related diseases. *Biogerontology* 2009;**10**:97−108.
28. Wu Q, Liu J, Mao ZG, Tian LY, Wang N, Wang GY, et al. Ligustilide attenuates ischemic stroke injury by promoting Drp1-mediated mitochondrial fission *via* activation of AMPK. *Phytomedicine* 2022;**95**:153884.
29. Wang M, Hayashi H, Horinokita I, Asada M, Iwatani Y, Liu JX, et al. Neuroprotective effects of Senkyunolide I against glutamate-induced cells death by attenuating JNK/caspase-3 activation and apoptosis. *Biomed Pharmacother* 2021;**140**:111696.
30. Han Y, Chen Y, Zhang Q, Liu BW, Yang L, Xu YH, et al. Overview of therapeutic potentiality of *Angelica sinensis* for ischemic stroke. *Phytomedicine* 2021;**90**:153652.
31. Miao WG, Nguyen T, Iqbal J, Pierens GK, Ma LL, Richardson DR, et al. Meeting the challenge 2: identification of potential chemical probes for Parkinson's disease from *Ligusticum chuanxiong* hort using cytological profiling. *ACS Chem Neurosci* 2022;**13**:2565−78.
32. Guo L, Gong MX, Wu S, Qiu F, Ma L. Identification and quantification of the quality markers and anti-migraine active components in Chuanxiong Rhizoma and Cyperi Rhizoma herbal pair based on chemometric analysis between chemical constituents and pharmacological effects. *J Ethnopharmacol* 2020;**246**:112228.
33. Xiao X, Zhang XX, Zhan MM, Cheng K, Li SY, Xie ZL, et al. Design, synthesis and bioevalucation of novel 2,3-dihydro-1*H*-inden-1-amine derivatives as potent and selective human monoamine oxidase B inhibitors based on rasagiline. *Eur J Med Chem* 2018;**145**:588−93.
34. Xiang HL, Zhang Q, Han YK, Yang L, Zhang Y, Liu Q, et al. Novel brain-targeting 3-*n*-butylphthalide prodrugs for ischemic stroke treatment. *J Control Release* 2021;**335**:498−514.
35. Su D, Zhang R, Wang X, Ding Q, Che FD, Zhang W, et al. A new multi-parameter imaging platform for *in vivo* drug efficacy evaluation of ischemic stroke. *Talanta* 2024;**266**:125133.
36. Yuan CL, Zheng L, Zhao YD. Protective effect of 3-n-butylphthalide against intrastriatal injection of malonic acid-induced neurotoxicity and biochemical alteration in rats. *Biomed Pharmacother* 2022;**155**:113664.
37. Mei YD, Pan DB, Jiang YN, Zhang WY, Yao XJ, Dai Y, et al. Target discovery of chlorogenic acid derivatives from the flower buds of Lonicera macranthoides and their MAO B inhibitory mechanism. *Fitoterapia* 2019;**134**:297−304.
38. Saleem U, Bibi S, Shah MA, Ahmad B, Saleem A, Chauhdary Z, et al. Anti-Parkinson's evaluation of *Brassica juncea* leaf extract and underlying mechanism of its phytochemicals. *Front Biosci-Landmark* 2021;**26**:1031−51.
39. Lalka D, Bardos TJ. Cyclophosphamide, 2,2-dimethylaziridines and other alkylating agents as inhibitors of serum cholinesterase. *Biochem Pharmacol* 1975;**24**:455−62.
40. Fowler JS, Volkow ND, Logan J, Wang G-J, Mac Gregor RR, Schlyer D, et al. Slow recovery of human brain MAO B after L-deprenyl (Selegeline) withdrawal. *Synapse* 1994;**18**:86−93.
41. Tipton KF, Boyce S, O'Sullivan J, Davey GP, Healy J. Monoamine oxidases: certainties and uncertainties. *Curr Med Chem* 2004;**11**:1965−82.
42. Prins LHA, Petzer JP, Malan SF. Inhibition of monoamine oxidase by indole and benzofuran derivatives. *Eur J Med Chem* 2010;**45**:4458−66.
43. Lees A. Alternatives to levodopa in the initial treatment of early Parkinson's disease. *Drugs Aging* 2005;**22**:731−40.
44. Wang MX, Chen JS, Zhang RR, Guo XY, Chen DX, Guo X, et al. Design, synthesis and bioactive evaluation of geniposide derivatives for antihyperuricemic and nephroprotective effects. *Bioorg Chem* 2021;**116**:105321.
45. Song Q, Yu GJ, Li W, Xu YD, Cong SQ, Liu XX, et al. 6-Benzyloxyphthalides as selective and reversible monoamine oxidase B inhibitors with antioxidant and anti-neuroinflammatory activities for Parkinson's disease treatment. *Bioorg Chem* 2022;**120**:105623.
46. Dong XW. Current strategies for brain drug delivery. *Theranostics* 2018;**8**:1481−93.
47. Yoon CH, Kim SJ, Shin BS, Lee KC, Yoo SD. Rapid screening of blood−brain barrier penetration of drugs using the immobilized artificial membrane phosphatidylcholine column chromatography. *SLAS Discovery* 2006;**11**:13−20.
48. Xicoy H, Wieringa B, Martens GJM. The SH-SY5Y cell line in Parkinson's disease research: a systematic review. *Mol Neurodegener* 2017;**12**:10.
49. De Medeiros LM, De Bastiani MA, Rico EP, Schonhofen P, Pfaffenseller B, Wollenhaupt-Aguiar B, et al. Cholinergic differentiation of human neuroblastoma SH-SY5Y cell line and its potential use as an *in vitro* model for Alzheimer's disease studies. *Mol Neurobiol* 2019;**56**:7355−67.
50. Yu ZR, Kong DW, Liang Y, Zhao XY, Du GH. Protective effects of VMY-2-95 on corticosterone-induced injuries in mice and cellular models. *Acta Pharm Sin B* 2021;**11**:1903−13.
51. Xie SS, Liu J, Tang CL, Pang CY, Li Q, Qin YL, et al. Design, synthesis and biological evaluation of rasagiline-clorgyline hybrids as novel dual inhibitors of monoamine oxidase-B and amyloid-β aggregation against Alzheimer's disease. *Eur J Med Chem* 2020;**202**:112475.
52. Reis J, Manzella N, Cagide F, Mialet-Perez J, Uriarte E, Parini A, et al. Tight-binding inhibition of human monoamine oxidase B by chromone analogs: a kinetic, crystallographic, and biological analysis. *J Med Chem* 2018;**61**:4203−12.
53. Tripathi RKP, Ayyannan SR. Monoamine oxidase-B inhibitors as potential neurotherapeutic agents: an overview and update. *Med Res Rev* 2019;**39**:1603−706.

54. Dhanabalan AK, Subaraja M, Palanichamy K, Velmurugan D, Gunasekaran K. Identification of a chlorogenic ester as a monoamine oxidase (MAO-B) inhibitor by integrating "traditional and machine learning" virtual screening and *in vitro* as well as *in vivo* validation: a lead against neurodegenerative disorders? *ACS Chem Neurosci* 2021; **12**:3690−707.
55. Mathew B, Adeniyi AA, Dev S, Joy M, Ucar G, Mathew GE, et al. Pharmacophore-based 3D-QSAR analysis of thienyl chalcones as a new class of human MAO-B inhibitors: investigation of combined quantum chemical and molecular dynamics approach. *J Phys Chem B* 2017;**121**:1186−203.
56. Matos MJ, Terán C, Pérez-Castillo Y, Uriarte E, Santana L, Viña D. Synthesis and study of a series of 3-arylcoumarins as potent and selective monoamine oxidase B inhibitors. *J Med Chem* 2011;**54**:7127−37.
57. Elkamhawy A, Kim HJ, Elsherbeny MH, Paik S, Park JH, Gotina L, et al. Discovery of 3,4-dichloro-N-(1*H*-indol-5-yl)benzamide: a highly potent, selective, and competitive hMAO-B inhibitor with high BBB permeability profile and neuroprotective action. *Bioorg Chem* 2021; **116**:105352.
58. Zhang XL, Liu LF, Zhu LY, Bai YJ, Mao Q, Li SL, et al. A high performance liquid chromatography fingerprinting and ultra high performance liquid chromatography coupled with quadrupole time-of-flight mass spectrometry chemical profiling approach to rapidly find characteristic chemical markers for quality evaluation of dispensing granules, a case study on Chuanxiong Rhizoma. *J Pharm Biomed Anal* 2014;**88**:391−400.
59. Zhu M, Duan JA, Tang YP, Guo JM, Shang EX, Zhu ZH. Identification of chemical constituents in SiWu decoction by UHPLC-DAD-TOF/MS. *Acta Chromatogr* 2014;**26**:517−37.
60. Wang YL, Fan SN, Yang M, Shi GX, Hu SY, Yin DK, et al. Evaluation of the mechanism of Danggui-Shaoyao-San in regulating the metabolome of nephrotic syndrome based on urinary metabonomics and bioinformatics approaches. *J Ethnopharmacol* 2020;**261**:113020.
61. Barcellos MP, Santos CBR, Federico LB, Almeida PFD, Da Silva CHTDP, Taft CA. Pharmacophore and structure-based drug design, molecular dynamics and admet/tox studies to design novel potential pad4 inhibitors. *J Biomol Struct Dyn* 2019;**37**:966−81.
62. Distinto S, Meleddu R, Yanez M, Cirilli R, Bianco G, Sanna ML, et al. Drug design, synthesis, *in vitro* and *in silico* evaluation of selective monoaminoxidase B inhibitors based on 3-acetyl-2-dichlorophenyl-5-aryl-2,3-dihydro-1,3,4-oxadiazole chemical scaffold. *Eur J Med Chem* 2016;**108**:542−52.
63. Binda C, Wang J, Pisani L, Caccia C, Carotti A, Salvati P, et al. Structures of human monoamine oxidase B complexes with selective noncovalent inhibitors: safinamide and coumarin analogs. *J Med Chem* 2007;**50**:5848−52.